Published in final edited form as:
Cancer Res. 2008 December 15; 68(24): 10257. doi:10.1158/0008-5472.CAN-08-0288.

Breast Cancer-associated Fibroblasts Confer AKT1-mediated Epigenetic Silencing of *Cystatin M* in Epithelial Cells

Huey-Jen L. Lin[*,1,2], **Tao Zuo**[*,1,2], **Ching-Hung Lin**[7], **Chieh Ti Kuo**[2], **Sandya Liyanarachchi**[2], **Shuying Sun**[3], **Rulong Shen**[4], **Daniel E. Deatherage**[2], **Dustin Potter**[2], **Lisa Asamoto**[1], **Shili Lin**[6], **Pearlly S. Yan**[2], **Ann-Lii Cheng**[7], **Michael C. Ostrowski**[5], and **Tim H.-M. Huang**[2]

[1]Division of Medical Technology, School of Allied Medical Professions, Comprehensive Cancer Center, The Ohio State University, Columbus, Ohio, USA

[2]Human Cancer Genetics Program, Comprehensive Cancer Center, The Ohio State University, Columbus, Ohio, USA

[3]Mathematical Biosciences Institute, Comprehensive Cancer Center, The Ohio State University, Columbus, Ohio, USA

[4]Department of Pathology, Comprehensive Cancer Center, The Ohio State University, Columbus, Ohio, USA

[5]Department of Molecular and Cellular Biochemistry, Comprehensive Cancer Center, The Ohio State University, Columbus, Ohio, USA

[6]Department of Statistics, Comprehensive Cancer Center, The Ohio State University, Columbus, Ohio, USA

[7]Department of Oncology, National Taiwan University Hospital, Taipei, Taiwan

Abstract

The interplay between histone modifications and promoter hypermethylation provides a causative explanation for epigenetic gene silencing in cancer. Less is known about the upstream initiators that direct this process. Here, we report that the *Cystatin M* (*CST6*) tumor suppressor gene is concurrently down-regulated with other loci in breast epithelial cells co-cultured with cancer-associated fibroblasts (CAFs). Promoter hypermethylation of *CST6* is associated with aberrant AKT1 activation in epithelial cells, as well as the disabled INNP4B regulator resulted from the suppression by CAFs. Repressive chromatin, marked by trimethyl-H3K27 and dimethyl-H3K9, and *de novo* DNA methylation is established at the promoter. The findings suggest that microenvironmental stimuli are triggers in this epigenetic cascade, leading to the long-term silencing of *CST6* in breast tumors. Our present findings implicate a causal mechanism defining how tumor stromal fibroblasts support neoplastic progression by manipulating the epigenome of mammary epithelial cells. The result also highlights the importance of direct cell-cell contract between epithelial cells and the surrounding fibroblasts that confer this epigenetic perturbation. Since this two-way interaction is anticipated, the described co-culture system can be used to determine the effect of epithelial factors on fibroblasts in future studies.

Requests for reprints: Tim H.-M. Huang, Phone: 614-688-8277; Fax: 614-292-5995; tim.huang@osumc.edu; or Huey-Jen L. Lin, Phone: 614-688-3088; Fax: 614-688-4181; huey-jen.lin@osumc.edu.

[*]Huey-Jen L. Lin and Tao Zuo contributed equally to this work.

Introduction

It is increasingly apparent that tumorigenesis depends not only on the acquisition of genetic alterations, but also on epigenetic perturbations that add an important layer of transcriptional control to the cancer genome. This type of alteration involves chemical modifications of DNA or histones that do not affect the nucleotide composition of cancer cells (1,2). To date, one well-characterized alteration is DNA methylation in which the cytosine residue of a CpG dinucleotide is converted into 5-methylcytosine by DNA methyltransferases (1,2). This chemical event frequently occurs in GC-rich sequences, known as CpG islands, located in 60–70% of the promoters or first exons of known genes (3). Increasing evidence has shown that *de novo* DNA methylation at 5'-end regulatory regions plays a causal role in maintaining silencing of tumor suppressor genes in solid tumors, including breast cancer (4). This hypermethylation is now linked and perhaps directly contributes to initiation, invasion, metastasis, and chemotherapeutic resistance of cancer cells (4,5).

In addition to promoter hypermethylation, regional modification of chromatin may render genes susceptible to silencing in cancer cells (4). These post-translational modifications, including acetylation, phosphorylation, ubiquitination, or methylation, occur primarily in the N-terminal tails of histones (6). Combinatorial alterations likely mark differential degrees of gene silencing, starting from a transient to a more rigid state of repression. Modification by methylation of histone H3 on lysine 27 may signify the target gene to undergo permanent silencing (7–9). This process is mediated by polycomb repressors that serve as a docking platform for DNA methyltransferases (10). Subsequent acquisition of DNA methylation may warrant an irrevocable state of silencing in the targeted gene. This epigenetic mark can be mitotically heritable in progeny cells (3).

While the causative interplay between DNA methylation and chromatin modifications is important in maintaining gene silencing, the upstream regulators that direct this epigenetic process are less known. Recent findings by our laboratory (11) and others (12) suggest that activation of oncogenic signaling may convey silencing of down-stream targets by epigenetic mechanisms. As an integrated entity within the tumor mass, the stromal microenvironment provides growth-promoting signals (13) that subsequently direct aberrant molecular changes in epithelial cells (13,14). Within the tumor stroma, cancer-associated fibroblasts (CAFs) are the most active secretory cells known to support epithelial transformation (15,16). Oncogene-expressing mammary epithelial cells developed faster growing tumors when mixed with CAFs than with normal fibroblasts (NFs) isolated from cancer-free breast tissues (13,17). Likewise, in an animal model, gain of neoplastic transformation was achieved only when stromal fibroblasts were previously exposed to the carcinogen *N*-nitrosomethylurea (18).

To determine whether CAFs can act as initiators orchestrating aberrant epigenomes, we developed an *in vitro* system in which an immortalized normal breast epithelial cell line, MCF10A (19), was co-cultured with CAFs or NFs isolated from different patient tissues. Expressional profiling of the resultant MCF10A identified concurrently down-regulated loci, including the newly characterized tumor suppressor *Cystatin M (CST6)* (20,21). Further analysis demonstrated that promoter hypermethylation and repressive chromatin states were established within the vicinity of the *CST6* CpG islands. This epigenomic perturbation was, in part, mediated by the activated serine/threonine kinase AKT1 signaling pathway in MCF10A cells. The proof-of-principle study demonstrates that epigenetically mediated gene silencing in epithelial cells can be influenced by neighboring fibroblasts. The co-culture system described here provides a practical approach for deciphering microenvironmental signals that re-program the epithelial epigenome.

Materials and Methods

Clinical samples

Breast tissue, from either tumors or cancer-free women undergoing reduction mammoplasty, was minced and dissociated enzymatically as described (22). The resultant single-cell mixture was subjected to centrifugation to segregate the fibroblast-enriched fraction from epithelial cells. Fibroblasts were collected and grown in F12/DMEM medium supplemented with 5% fetal bovine serum (FBS) and insulin (5 μg/ml). The immunofluorescence staining was employed to confirm two hallmark fibroblastic antigens: vimentin (13,23) (NCL-L-VIM-V9; Novocastra Laboratories, Ltd., United Kingdom) and prolyl-4-hydroxylase (13) (ab39342; Abcam). The use of human breast tissues samples was approved by the Institutional Review Boards of the Ohio State University and the National Taiwan University Hospital. Macrodissected tumor and cancer-free samples were used for immunostaining and DNA isolation.

Co-culture of breast fibroblasts with MCF10A cells

The spontaneously immortalized but non-cancerous breast epithelial cell line, MCF10A (19, 24), was grown in F-12 medium containing FBS (5%), insulin (5 μg/ml), cholera toxin (100 ng/ml), hydrocortisone (1 μg/ml), hEGF (10 ng/ml), penicillin (100 units/ml) and streptomycin (100 μg/ml). Fibroblasts (6×10^5) were mixed with MCF10A cells (4×10^5) and overlaid on the Matrigel-precoated cultivation vessels (BD Biosciences) in serum-free medium supplemented with defined growth factors, namely hEGF (10 ng/ml) and bFGF (20 ng/ml) (17). Such combinatorial 2-dimensional culture, known as co-culture, was maintained for an additional 21 days with media changes 3 times per week. This time duration was determined by 1) cell confluence on a plate; and 2) the deterioration of Matrigel after 21 days on culture dishes (informed by the manufacturer).

A study was also conducted by pre-labeling MCF10A with a tracking dye (CFDA, V12883, Invitrogen) prior to co-culturing these cells with fibroblasts. The distribution of different cell populations was then monitored in culture dishes. MCF10A cells were in full contact with fibroblasts at a ratio of 1.5 (fibroblasts: MCF10A). This initial ratio (Fig. 4C) was adequate to confer a co-culture effect though the proportion of fibroblasts seemed to be higher than that was observed in breast tissue sections (Fig. 1A and 6B). However, we experienced that fibroblasts usually grow slower than MCF10A cells in culture dishes. Therefore, the eventual ratio of fibroblasts to MCF10A cells in this co-culture system might resemble those observed *in vivo*.

Cell sorting

Co-cultured MCF10A cells were purified from cell mixture by immunofluorescence staining followed by flow cytometric sorting. Briefly, cells were detached from the Matrigel mediated by dispase (BD Biosciences), and then the cell-cell junctions were broken down by trypsin cleavage. Single cell population was assured by sieving through 100 μm Cell Strainer (BD Biosciences). Filtered cells were subjected to immunofluorescence staining using a FITC-conjugated antibody recognizing ESA (Epithelial Specific Antigen; FM010; Biomeda). After 30 minutes of incubation on ice followed by extensive washing with HBSS plus 5% FCS, the resultant cells were stained with 7-AAD to exclude dead cells. Four additional controls were employed to serve as gating cutoffs for flow cytometric sorting. This was MCF10A alone (minus fibroblasts) or fibroblasts alone (minus MCF10A), stained with either ESA or with an isotypic negative control antibody. The cells that retained $ESA^+/7AAD^-$ properties were collected from FACSAria while the dead cells and contaminating fibroblasts were discarded. Small aliquots of purified MCF10A cells were cultured to ascertain the epithelial originality (>99% purity), assessed by the presence of the epithelial-specific marker ESA. The purified

MCF10A cells were divided into two equal fractions for RNA and DNA extractions, respectively.

Gene expression microarray

Total RNA, extracted from cells of interest by using TRIZOL reagent (Invitrogen), was used for microarray hybridization with the Affymetrix U133 plus 2.0 chip system (Affymetrix, Santa Clara, CA). The quantitative estimates of gene expression array were generated using the Robust Multichip Average (RMA) algorithm with background correction and quantile normalization (25). Statistical software package R (http://www.r-project.org/) with bioconductor package Affy was used to obtain RMA estimates. Any effect of different microarray processing was removed using Batch Removal tool of Partek Genomic Suite 6.3 (Partek Inc, St. Charles, MO) software. To identify genes that were differentially expressed in co-cultured MCF10A cells, an unpaired two class comparison was performed using the Significance Analysis of Microarrays (SAM) algorithm (26). SAM is a method based on repeated permutations that controls false discovery rate (FDR) to adjust for multiple testing. Initial filtering of the probe sets was conducted by controlling FDR at 0.89% level and with a 2-fold change in the comparison between the test and control groups. The initial list was further filtered by considering probes that showed reduce gene expression in MCF10A cells exposed to CAFs compared to the mock control. Hierarchical cluster analysis of the samples was performed with Pearson correlation similarity metric and average linkage method using R software. The resultant microarray data were submitted to NCBI Gene Expression Omnibus database with an accession number of GSE10046.

Assessment of DNA methylation by MassARRAY

To quantify the methylation level of the CpG sites of *CST6*, we carried out a high-throughput methylation assay known as MassARRAY (Sequenom, Inc.). This system utilizes mass spectrometry for the detection and quantifying DNA methylation using the homogeneous MassCLEAVE base-specific cleavage and matrix-assisted laser desorption/ionization time-of-flight MS (27). Briefly, genomic DNA (1 μg) was converted with sodium bisulfite and subjected to PCR reactions to amplify a region to be analyzed. Each reverse primer encompasses a T7-promotor tag for a subsequent *in vitro* transcription. After the alkaline phosphatase treatment, PCR products were used as a template for *in vitro* transcription followed by RNase A cleavage for the T-reverse reactions. The products were spotted on a 384-pad SpectroCHIP (Sequenom, Inc.) followed by spectral acquisition on a MassARRAY Analyzer. The methylation calls were performed by the EpiTyper software v1.0 (Sequenom Inc.), which generates quantitative results for each CpG site or an aggregate of multiple CpG sites.

Immunofluorescence staining and image quantification

Fibroblasts (3×10^3) were co-cultured with MCF10A cells (2×10^3) in a matrigel-precoated 8-well chamber slide (354118, BD Falcon). Two weeks later, cells were fixed with 2% paraformaldehyde followed by permeablization with 0.5% Triton X-100 containing cocktail phosphatase inhibitors (1mM sodium orthovanadate, 10mM sodium fluoride, and 10mM β-glycerophosphate, G6376, Sigma). The resultant cells were treated with 10% goat serum to block non-specific antigens, and followed by an incubation with a mixture of anti-phospho-AKT1 (Ser 473) rabbit antibody (9271, Cell Signaling Technology, dilution 1:100) and FITC-conjugated anti-ESA antibody (FM010; Biomeda; dilution 1:200) at 4°C for an overnight. Cells were further incubated with Texas-Red conjugated goat-anti-rabbit IgG (TI-1000, Vector Laboratories, dilution 1:200) to visualize the immunocomplexes of the former antibody, followed by a staining with DAPI (P-36931, Invitrogen) to localize cell nuclei. Final image, captured by a confocal laser scanning microscope (Zeiss LSM 510), was quantified by a custom-written macro in the Image Pro® Plus software v6.3 (Media Cybernetics, Inc.

Bethesda, MD http://mediacy.com/). Green and red signals were individually captured as areas of interest (AOI) in separate images. After normalization, each image was converted to an 8-bit gray scale. Based on the AOI of a given image, the areas resulted from red and green signals were measured in pixels and were converted into number of cells that exerted respective signals.

AKT1 transfection and kinase activity assay

Either a vehicle control or a pCDNA3 plasmid encoding *MyrAKT1* (28) (1036; Addgene), which expresses a constitutively active AKT1, was transfected into MCF10A cells by LipofectAMINE Plus (Invitrogen). Seventy-two hours later, transfected cells were propagated in growth media supplemented with geneticin (G418, 400 μg/ml, Invitrogen). Survival colonies were pooled for subsequent studies. To measure kinase activities of the *MyrAKT1* transfectants, AKT1 (in the crude cell lysate) was precipitated by a specific antibody that recognizes the Pleckstrin Homology domain without interfering with its kinase activity (ST1088; Calbiochem). The immune-complexes were then incubated with a biotinylated peptide substrate, which became phosphorylated in the presence of activated AKT1. The phosphorylated substrates, directly reflected the level of AKT1 kinase in the cell extract, was quantified by the K-LISA AKT Activity Kit (CBA019; Calbiochem) comprising a primary antibody recognizing the phosphorylated substrate peptides.

Chromatin immunoprecipitation (ChIP)-PCR

ChIP was carried out as described previously (29). Briefly, cells grown at sub-confluent logarithm phase were fixed with 1% formaldehyde, a reagent cross-linking proteins to DNA. The resultant DNA-protein complexes were sonicated followed by immunoprecipitation using Dynabeads Protein G (100.04D; Invitrogen) coated with control IgG antibody or with a respective antibody recognizing protein of interest. Four antibodies used to analyze chromatin marks or DNMT1 were anti-trimethyl-H3K27 (07-449; UpState), anti-dimethyl-H3K9 (ab7312-100; Abcam), anti-acetyl-H3K9 (06-599; UpState), and anti-DNMT1 (IMG-261A; IMGeneX). The DNA fragments were later dissociated from the immunocomplexes, and the amount of amplified products was quantified by real-time PCR. Normalization of pull downs was carried out by comparing with the initial input DNA prior to the immunoprecipitation treatment. ChIP-PCR primers were listed in Supplementary Table S5.

Immunohistochemical staining

To detect phospho-AKT1, immunohistochemical studies were performed on available paraffin sections from 72 tissue samples using an indirect biotin-avidin method. Sections were cut at 5μm thickness, deparaffinized and rehydrated. Endogenous peroxidase activity was blocked with hydrogen peroxide/methanol, and antigen retrieval was performed in a pH6.0 buffer (CMX833-C, Triology, Rocklin) by autoclave for 10 min. The resultant tissue sections were then incubated with rabbit P-Akt (Ser 473) monoclonal antibody (Clone 736E11; Cell Signaling Technology; dilution, 1:20) at 4°C overnight. Immunocomplexes were visualized by using the iView DAB detection system (Nexus IHC, Ventana Medical Systems, Tucson). A slide with paraffin-embedded Jukart cells was used as a positive control. The intensity score was determined by two viewers with the following criteria: 0 = no appreciable staining in the tumor cells, 1 = barely detectable staining in the cytoplasm and/or nucleus compared with the stromal elements, 2 = readily appreciable brown staining distinctly marking the tumor cell cytoplasm and/or nucleus, 3 = dark brown staining in tumor cells obscuring the cytoplasm and/or nucleus, or 4 = very strong staining of nucleus and/or cytoplasm. After assigning a fraction score to a given tissue to reflect the fraction of positive cells (0–100%), the total score was calculated by multiplying the intensity score and the fraction score producing a total range between 0 and 400. For statistical analyses, tumors with scores of 0–200 were categorized as negative/low expressors, while the ones with scores of 201–400 were positive/high.

Statistical analysis

The Student's *t*-test was conducted to analyze significance of data derived from quantitative real-time RT-PCR, ChIP-PCR, and MassARRAY methylation assays. A significance was assigned if $p < 0.05$. Logistic regression was used to analyze the expression correlation between *CST6* and *INPP4B*.

Results

In vitro co-culture system revealed microenvironmental influences on epithelial gene silencing

As breast stromal cells are usually situated in close contact with the tumor core (Fig. 1A and 6B), we postulated that surrounding fibroblasts play a role in re-programming of the epithelial epigenome. To test this model, we developed a co-culture system to simulate the physical interaction between epithelial cells and fibroblasts *in vivo*. CAFs were isolated from 12 breast tumors. NFs were isolated from 8 cancer-free tissues from women undergoing reduction mammoplasty (Fig. 1B and Supplementary Table S1). Greater than 98% of these primary cells exhibited fibroblastic characteristics as confirmed by immunofluorescence staining to detect two markers, vimentin and prolyl-4-hydroxylase (13,23,30) (Fig. S1). Co-cultures comprised of an individual CAF or NF (≤5 passages) and MCF10A were then employed in a Matrigel-containing culture system (17). Three weeks later, 1–2 million cells were sorted by a flow cytometer using an antibody against human epithelial-specific antigen (ESA) (Fig. 1C). In general, the resultant cell fraction retained 99% purity of MCF10A cells as confirmed by their reactivity to the ESA antibody.

Global expression profiling of co-cultured MCF10A cells was carried out to identify down-regulated genes instructed by CAFs. Five sets of co-cultured MCF10A cells (exposed to fibroblasts, C4, C12, C15, N16, and N23, respectively) and a mock control (i.e., MCF10A cells omitting any fibroblast exposure) were subjected to expression analysis. A total of 109 genes (Supplementary Table S2) were concurrently down-regulated in MCF10A co-cultured with CAFs relative to the counterpart exposed to NFs or the mock control. Among these genes, 56 loci harboring promoter CpG islands were shown in a heat map (Fig. 2). The hypermethylation status of 9 candidate genes was evaluated and confirmed in co-cultured MCF10A cells by methylation-specific PCR (Fig. S2).

Cell-cell contact between MCF10A and CAFs is essential for epithelial silencing of *CST6*

Hypermethylation of one candidate gene, *CST6*, was previously reported in breast cancer cell lines, primary and metastasized tumors (20,21). This gene has been shown to be a tumor suppressor, and is silenced by CpG island hypermethylation in breast cancer (20,21). We therefore conducted detailed methylation mapping of a 310-bp region located within the *CST6* CpG island in a collection of MCF10A samples exposed to various fibroblasts (n=20). Using quantitative MassARRAY, the methylation levels of this region were found to be significantly elevated in MCF10A cells upon exposure to different CAFs, as opposed to those co-cultured with NFs or mock control (p=0.026, t-test) (Fig. 3A and C). Moreover, hypermethylation was prominent in the region flanking the transcription start site of *CST6* (p=0.007, the underlined region shown in Fig. 3A). This finding was consistent with the data generated by bisulfite sequencing analysis of cloned PCR products (Fig. S3).

To determine whether increased methylation coincided with the down-regulation of *CST6*, we conducted quantitative RT-PCR in 12 of the aforementioned samples and the mock control (Fig. 3D). Regression analysis revealed an inverse relationship between the level of promoter methylation and copy number of the *CST6* transcript (p=0.005). This result suggests that

induced promoter methylation is correlated with *CST6* silencing in MCF10A cells, as a result of exposure to CAFs.

To exclude the possibility of contaminating fibroblasts as a source for the observed hypermethylation, we determined the methylation status of *CST6* in corresponding fibroblasts (without the co-culture treatment) by MassARRAY (Fig. 3B). The level of *CST6* methylation in CAFs or NFs was generally lower than MCF10A cells co-cultured with CAFs (Fig. 3C). Because negligible *CST6* promoter methylation was observed in the parental MCF10A as well as in fibroblasts, we suggest that elevated methylation observed in CAF-co-cultured MCF10A most likely resulted from a *de novo* event (Fig. 3A–C and S5), rather than from contaminating CAFs that would have otherwise underscored the methylation readout.

To evaluate whether soluble factors released from fibroblasts (without cell-cell contact) could induce *CST6* methylation, two additional experiments were undertaken. MCF10A cells were either continuously treated with fresh conditioned media (harvested from CAF or NF culture media), or directly exposed to soluble factors secreted from fibroblasts and passed on to MCF10A *via* a transwell system in the absence of cell-cell contact. Three weeks later, DNA extracted from MCF10A cells was subjected to methylation analysis. Compared to the mock control, methylation alteration was negligible in MCF10A cells treated with either conditioned media (lower panel, Fig. 3B), or with transwell (data not shown). These data suggests that cell-cell contact is necessary for *de novo CST6* methylation.

CAFs trigger epithelial activation of AKT1 signaling that subsequently results in methylation-mediated silencing of *CST6*

To address which epithelial signaling pathway might be activated by CAFs that leads to *CST6* methylation, logistic regression was used to analyze expression microarray data derived from the aforementioned 5 sets of co-cultured samples and the mock control. Data were randomly permuted with replacement, from which the Spearman rank coefficient (SRC) was computed. This was repeated one million times providing an empirical estimate of the SRC distribution for the observed data. The resulting standard deviation was then used to determine a threshold of significance. Candidate loci whose expression were positively correlated with the expression level of *CST6* were further confirmed by a bootstrapping approach (31). Among genes with SRC≥2 (standard deviations from zero), we uncovered *INPP4B* (Inositol polyphosphate-4-phosphatase, type II), which encodes for a negative modulator of AKT1 kinase. Quantitative RT-PCR was then conducted to quantify its transcript in co-cultured samples (n=13) and confirmed a positive correlation between the expression of *CST6* and *INPP4B* (SRC=0.71; p=0.004) (Fig. 4A). Aberrant activation of AKT1 signaling is known to be a frequent event in breast cancer (28,32,33) and is similarly observed in epithelial cells exposed to CAFs (current study). Dual immunofluorescence analysis showed the co-localization of ESA and phospho-AKT1 kinase in MCF10A cells exposed to CAFs, but not to NFs (Fig. 4B and 4C). This occurrence was influenced by the number of CAFs that were in contact with MCF10A cells. At a minimum ratio of 1.5 (fibroblasts: MCF10A), but not at lower ratios or in control NFs, phospho-AKT1 was remarkably increased (Fig. 4C). Taken together, these results indicate that activated AKT1 signaling is likely one of the causes leading to aberrant methylation of *CST6* in epithelial cells.

To investigate whether ectopical expression of phospho-AKT1 kinase in MCF10A cells could lead to the similar epigenetic perturbation observed in *CST6*, MCF10A cells were stably transfected with a vector expressing a constitutively active myristylated form of *AKT1* or an empty vehicle (34). An increased level (>42-fold) of *AKT1* mRNA, along with elevated kinase activity (>3-fold), was observed in the *AKT1*-transfected cells relative to that of the vector control (Fig. 4D). Interestingly, drastically decreased levels of both *INPP4B* and *CST6* mRNAs were seen in the same *AKT1* transfectants. While the *INPP4B* repression was likely due to a

negative feedback loop commanded by AKT1, activation of this signaling might lead to down-regulation of its target genes, such as *CST6*. Resulting from this constitutive suppression, a repressive chromatin might be established in the *CST6* CpG island. In support of this notion, ChIP-PCR assays demonstrated a 4- to 10-fold enrichment of 2 repressive chromatin marks (trimethyl-H3K27 and dimethyl-H3K9), but not an active mark (acetyl-H3K9), in the *CST6* promoter (Fig. 5A). Likewise, DNA methyltransferase 1 was found to be recruited to this region, resulting in an increase of *de novo* DNA methylation in the *CST6* promoter (Fig. 5A and B). This transfection study suggests that epigenetic silencing of *CST6* is mediated, in part, by activated AKT1 signaling in epithelial cells. Extending this notion, we further speculate that extracellular signaling initiated by CAFs can activate this oncogenic pathway and subsequently confer the epigenetic silencing of AKT1 target genes in neighboring epithelial cells.

Promoter hypermethylation of *CST6* is associated with phospho-AKT1 in primary breast tumors

To substantiate the *in vitro* findings, we conducted methylation analyses of the *CST6* CpG island in 194 primary breast tumors and 28 normal breast tissues by MassARRAY. The clinicopathological characteristics of these patients are provided in supplementary Table S3. In close agreement with the previous reports (20,21,35), ~25% of the analyzed tumors exhibited elevated levels of methylation in the core CpG island region (i.e., CpG sites 5 to 13) (Fig. 6A). Noticeably, CpG sites located on the outer flanks were more methylated in primary tumors than in normal controls. Consistent with the methylation spread theory (36), this *de novo* methylation may begin at the flanking regions and progressively invade to the core of the *CST6* CpG island in a given tumor.

Available clinicopathological information, including hormone receptor status, age at diagnosis, clinical staging, and histology grade, was also inferred to the epigenetic study. Among them, the intensity of phospho-AKT1 was found to be positively correlated with the hypermethylation of *CST6* (p=0.02, Fig. 6C). The result obtained from immunohistochemical staining of phospho-AKT1 in breast tumors (n=72) has revealed that tumors with high degrees of phospho-AKT1 generally bear great levels of methylation in the epithelia and are densely surrounded by fibroblasts (Fig. 6B). Taken together, the evidence from *in vitro* co-culture and from breast tumors consistently demonstrates that cell-cell contact may be an important contributor to AKT1 signaling pathway, which subsequently leads to aberrant *CST6* methylation.

Discussion

The present findings provide initial evidence that epigenetically mediated gene silencing in the epithelial genome can be directed by neighboring fibroblasts. In a combinatorial setting, a single breast epithelial cell line was in direct contact with different primary fibroblasts isolated from breast cancer patients or from cancer-free women. Variability in primary fibroblasts was expected because these cells were derived from women with different genetic backgrounds, life styles, daily diets, menopausal status, and ages. This heterogeneity indeed caused a wide spectrum of expression changes in MCF10A cells exposed to different primary fibroblasts (data not shown). However, further analysis of microarray data captured commonly dysregulated genes in co-cultured samples. We then determined the methylation status of some of these loci, including *CST6*, which were concurrently down-regulated in many MCF10A sets tested. This type of microarray analysis is also useful for deciphering common gene signatures or signaling pathways in different primary fibroblasts that may exert common influences on neighboring epithelial cells.

Our finding has further demonstrated that the epigenetically mediated silencing of *CST6* is, in part, governed by an activated AKT pathway, presumably in response to microenvironmental

stimuli. Whether the suppression of *CST6* is a direct or a secondary outcome of this signaling cascade remains to be determined. Nevertheless, three lines of experimental evidence suggest that promoter hypermethylation of *CST6* is a consequence of aberrant AKT1 kinase activation. First, immunofluorescence staining of co-cultured MCF10A revealed remarkable AKT1 activation after exposure to CAFs (Fig. 4B). Second, ectopical expression of AKT1 kinase in MCF10A cells conveyed *CST6* hypermethylation (Fig. 5B). Lastly, phospho-AKT1 was positively correlated with increased levels of *CST6* methylation in primary tumors (Fig. 6C). We have also found that in addition to PTEN, INPP4B may be an important negative regulator of AKT1 in breast epithelial cells (Fig. 4A). Future studies can determine whether dysregulation of INPP4B is also a frequent event in breast tumors with activated AKT1.

It is possible that CAFs support a proliferative advantage of an epithelial subpopulation that harbors pre-existing *CST6* methylation. Previous studies showed that hypermethylation of the *p16* promoter conveyed a clonal outgrowth of primary human mammary epithelial cells (HMECs), which would otherwise undergo senescence (37,38). However, this may not be the case in our study. First, unlike primary HMECs that comprise a mixture of epithelial cells, MCF10A is an immortalized line with minimal cellular heterogeneity. Second, no pre-existing *CST6* methylation was detectable in the parental MCF10A line (see the mock examples in Fig. 3A, C, S3 & S5). Third, after exposure to various CAFs (n=12), co-cultured MCF10A cells did not show noticeable methylation fingerprints of individual CpG sites presumably derived from a single clone. These results suggest that hypermethylation of *CST6* is unlikely the result of a clonal outgrowth of MCF10A cells. Nevertheless, to exclude the possibility of enrichment of a subpopulation, further studies by co-cultivating various “recloned” MCF10A cells with CAFs followed by *CST6* methylation analysis will be undertaken and should substantiate our current finding.

While the current study focuses on identifying epigenetic perturbations in epithelial cells exposed to neighboring fibroblasts, two-way interactions between these cell types are anticipated. In this regard, Polyak and colleagues (39) have recently uncovered widespread epigenetic alterations in cancer fibroblasts. It is tempting to speculate that malignant epithelial cells also play a role in directing epigenetic changes in stromal fibroblasts. To examine this possibility, a similar combinatorial approach can be performed by co-culturing different transformed epithelial cells with hTERT-immortalized (23) or primary fibroblasts. Microarray analysis could be used to identify common epigenetic perturbations in normal fibroblasts co-cultured with different neoplastic epithelial cells. Such a study can also be used to determine which oncogenic factors can be activated in the exposed fibroblast line.

It should be noted that CAFs are not “malignant” themselves and, in our hands, undergo senescence after limited passages (~10) in cell culture. At present, it is not known whether MCF10A cells will gain malignant phenotypes after exposure to primary CAFs. Future experiments can be conducted in a humanized xenograft model in which the development of human mammary glands is recapitulated by implanting both immortalized human fibroblasts and breast epithelial cells in cleared mouse mammary fat pads (23). This “human-in-mouse” model would provide a better physiological environment to investigate epigenetic perturbations influenced by tumor microenvironment and thus validate our current findings.

While our results suggest CAFs alone are sufficient to cause epithelial silencing of particular loci, tumor microenvironment is far more complex. It contains not only fibroblasts, but also many different cell types, including infiltrating lymphocytes, macrophages and endothelial cells. Collections of bioactive molecules released from various stromal cell types in the tumor milieu may synergistically confer epigenetic alterations and promote tumorigenesis (15–17, 40). Depending on particular cell types within a given microenvironment, complex cell-cell interactions are proposed to be critical in triggering epigenetically mediated gene silencing in

epithelial cells. Accumulating experimental evidence has indeed supported this premise. Chung *et al.* (41) found that hypermethylation of *CYP24* occurred only if endothelial cells were directly exposed to an *in vivo* tumor microenvironment. However, this methylation was not observed when endothelial cells were exposed to conditioned media obtained from cancer cells (42). Consistent with this finding, our result demonstrates that *CST6* methylation could only be induced if MCF10A cells were in direct contact with fibroblasts in culture, but not by conditioned medium treatments or by transwell co-culture. Likely, complex alterations will be better understood by using new co-culture systems that accommodate additional cell types (other than fibroblasts) for measuring the synergistic effect of cell-cell interaction on epigenetic gene silencing.

In summary, this proof-of-principle study supports the hypothesis that microenvironmental factors are triggers of epigenetic gene silencing in the epithelial genome. In combinatorial settings, different cell types can be mixed together in a co-culture system. Methylation analysis can then be conducted in the desired cell type purified by flow cytometry or magnetic bead separation. Future use of this co-culture approach will provide an unprecedented opportunity to study cell-cell interaction and its influence on epigenetically mediated gene silencing.

Acknowledgments

This work was supported by NIH grants (U54CA113001 and R01CA069065), funds from American Cancer Society, Department of Defense (BC073892), Susan G. Komen Breast Cancer Foundation (KG081123), and the Ohio State University Comprehensive Cancer Center. D.P. and S.S. were supported by the NIH (T32 CA106196-03) and the National Science Foundation (#0112050) post-doctoral fellowships, respectively. We thank Mrs. Xiaoping Liu, Mr. Paul Ladipo, and Drs. Michael W. Y. Chan, Jiejun Wu, Chang Gong Liu, Hansjuerg Alder, Xiang Au, Bryan Mc Elwain, Alan Bakaletz and Kurtis H. Yearsley for their technical assistance; and Mr. Benjamin Rodriguez for critical reading of this manuscript.

References

1. Callinan PA, Feinberg AP. The emerging science of epigenomics. Hum Mol Genet 2006;1:95–101.
2. Fuks F. DNA methylation and histone modifications: teaming up to silence genes. Curr Opin Genet Dev 2005;15:490–495. [PubMed: 16098738]
3. Antequera F, Bird A. CpG islands as genomic footprints of promoters that are associated with replication origins. Curr Biol 1999;9:661–667. [PubMed: 10375532]
4. Jones PA, Baylin SB. The epigenomics of cancer. Cell 2007;128:683–692. [PubMed: 17320506]
5. Plimack ER, Stewart DJ, Issa JP. Combining epigenetic and cytotoxic therapy in the treatment of solid tumors. J Clin Oncol 2007;25:4519–4521. [PubMed: 17925545]
6. Ting AH, McGarvey KM, Baylin SB. The cancer epigenome--components and functional correlates. Genes Dev 2006;20:3215–3231. [PubMed: 17158741]
7. Lachner M, O'Sullivan RJ, Jenuwein T. An epigenetic road map for histone lysine methylation. J Cell Sci 2003;116:2117–2124. [PubMed: 12730288]
8. Gibbons RJ. Histone modifying and chromatin remodelling enzymes in cancer and dysplastic syndromes. Hum Mol Genet 2005;141:85–92.
9. McGarvey KM, Greene E, Fahrner JA, Jenuwein T, Baylin SB. DNA methylation and complete transcriptional silencing of cancer genes persist after depletion of EZH2. Cancer Res 2007;67:5097–5102. [PubMed: 17545586]
10. Vire E, Brenner C, Deplus R, et al. The Polycomb group protein EZH2 directly controls DNA methylation. Nature 2006;439:871–874. [PubMed: 16357870]
11. Leu YW, Yan PS, Fan M, et al. Loss of estrogen receptor signaling triggers epigenetic silencing of downstream targets in breast cancer. Cancer Res 2004;64:8184–8192. [PubMed: 15548683]
12. Ren M, Pozzi S, Bistulfi G, Somenzi G, Rossetti S, Sacchi N. Impaired retinoic acid (RA) signal leads to RARbeta2 epigenetic silencing and RA resistance. Mol Cell Biol 2005;25:10591–10603. [PubMed: 16287870]

13. Orimo A, Gupta PB, Sgroi DC, et al. Stromal fibroblasts present in invasive human breast carcinomas promote tumor growth and angiogenesis through elevated SDF-1/CXCL12 secretion. Cell 2005;121:335–348. [PubMed: 15882617]

14. Tlsty TD, Coussens LM. Tumor stroma and regulation of cancer development. Annu Rev Pathol 2006;1:119–150. [PubMed: 18039110]

15. Bhowmick NA, Neilson EG, Moses HL. Stromal fibroblasts in cancer initiation and progression. Nature 2004;432:332–337. [PubMed: 15549095]

16. Kalluri R, Zeisberg M. Fibroblasts in cancer. Nat Rev Cancer 2006;6:392–401. [PubMed: 16572188]

17. Shekhar MP, Werdell J, Santner SJ, Pauley RJ, Tait L. Breast stroma plays a dominant regulatory role in breast epithelial growth and differentiation: implications for tumor development and progression. Cancer Res 2001;61:1320–1326. [PubMed: 11245428]

18. Maffini MV, Soto AM, Calabro JM, Ucci AA, Sonnenschein C. The stroma as a crucial target in rat mammary gland carcinogenesis. J Cell Sci 2004;117:1495–1502. [PubMed: 14996910]

19. Soule HD, Maloney TM, Wolman SR, et al. Isolation and characterization of a spontaneously immortalized human breast epithelial cell line, MCF-10. Cancer Res 1990;50:6075–6086. [PubMed: 1975513]

20. Ai L, Kim WJ, Kim TY, et al. Epigenetic Silencing of the Tumor Suppressor Cystatin M Occurs during Breast Cancer Progression. Cancer Res 2006;66:7899–7909. [PubMed: 16912163]

21. Rivenbark AG, Livasy CA, Boyd CE, Keppler D, Coleman WB. Methylation-dependent silencing of CST6 in primary human breast tumors and metastatic lesions. Exp Mol Pathol 2007;83:188–197. [PubMed: 17540367]

22. Stingl J, Eaves CJ, Kuusk U, Emerman JT. Phenotypic and functional characterization in vitro of a multipotent epithelial cell present in the normal adult human breast. Differentiation 1998;63:201–213. [PubMed: 9745711]

23. Kuperwasser C, Chavarria T, Wu M, et al. Reconstruction of functionally normal and malignant human breast tissues in mice. Proc Natl Acad Sci U S A 2004;101:4966–4971. [PubMed: 15051869]

24. Soule HD, McGrath CM. A simplified method for passage and long-term growth of human mammary epithelial cells. In Vitro Cell Dev Biol 1986;22:6–12. [PubMed: 2418007]

25. Bolstad BM, Irizarry RA, Astrand M, Speed TP. A comparison of normalization methods for high density oligonucleotide array data based on variance and bias. Bioinformatics 2003;19:185–193. [PubMed: 12538238]

26. Tusher VG, Tibshirani R, Chu G. Significance analysis of microarrays applied to the ionizing radiation response. Proc Natl Acad Sci U S A 2001;98:5113–5121.

27. Ehrich M, Zoll S, Sur S, van den Boom D. A new method for accurate assessment of DNA quality after bisulfite treatment. Nucleic Acids Res 2007;35:29–37.

28. Ramaswamy S, Nakamura N, Vazquez F, et al. Regulation of G1 progression by the PTEN tumor suppressor protein is linked to inhibition of the phosphatidylinositol 3-kinase/Akt pathway. Proc Natl Acad Sci U S A 1999;96:2110–2115. [PubMed: 10051603]

29. Cheng AS, Jin VX, Fan M, et al. Combinatorial analysis of transcription factor partners reveals recruitment of c-MYC to estrogen receptor-alpha responsive promoters. Mol Cell 2006;21:393–404. [PubMed: 16455494]

30. Kim JB, Stein R, O'Hare MJ. Tumour-stromal interactions in breast cancer: the role of stroma in tumourigenesis. Tumour Biol 2005;26:173–185. [PubMed: 16006771]

31. Harrell, J. F.E. Regression Modeling Strategies: With Applications to Linear Models, Logistic Regression, and Survivial Analysis. New York: Springer; 2001. p. 90-97.

32. Barnache S, Le Scolan E, Kosmider O, Denis N, Moreau-Gachelin F. Phosphatidylinositol 4-phosphatase type II is an erythropoietin-responsive gene. Oncogene 2006;25:1420–1423. [PubMed: 16247441]

33. Altomare DA, Testa JR. Perturbations of the AKT signaling pathway in human cancer. Oncogene 2005;24:7455–7464. [PubMed: 16288292]

34. Priore R, Dailey L, Basilico C. Downregulation of Akt activity contributes to the growth arrest induced by FGF in chondrocytes. J Cell Physiol 2006;207:800–808. [PubMed: 16523491]

35. Rivenbark AG, Jones WD, Coleman WB. DNA methylation-dependent silencing of CST6 in human breast cancer cell lines. Lab Invest 2006;86:1233–1242. [PubMed: 17043665]

36. Stirzaker C, Song JZ, Davidson B, Clark SJ. Transcriptional gene silencing promotes DNA hypermethylation through a sequential change in chromatin modifications in cancer cells. Cancer Res 2004;64:3871–3877. [PubMed: 15172996]

37. Brenner AJ, Stampfer MR, Aldaz CM. Increased p16 expression with first senescence arrest in human mammary epithelial cells and extended growth capacity with p16 inactivation. Oncogene 1998;17:199–205. [PubMed: 9674704]

38. Romanov SR, Kozakiewicz BK, Holst CR, Stampfer MR, Haupt LM, Tlsty TD. Normal human mammary epithelial cells spontaneously escape senescence and acquire genomic changes. Nature 2001;409:633–637. [PubMed: 11214324]

39. Hu M, Yao J, Cai L, et al. Distinct epigenetic changes in the stromal cells of breast cancers. Nat Genet 2005;37:899–905. [PubMed: 16007089]

40. Nelson CM, Bissell MJ. Of extracellular matrix, scaffolds, and signaling: tissue architecture regulates development, homeostasis, and cancer. Annu Rev Cell Dev Biol 2006;22:287–309. [PubMed: 16824016]

41. Chung I, Karpf AR, Muindi JR, et al. Epigenetic silencing of CYP24 in tumor-derived endothelial cells contributes to selective growth inhibition by calcitriol. J Biol Chem 2007;282:8704–8714. [PubMed: 17244627]

42. Hellebrekers DM, Melotte V, Vire E, et al. Identification of epigenetically silenced genes in tumor endothelial cells. Cancer Res 2007;67:4138–4148. [PubMed: 17483324]

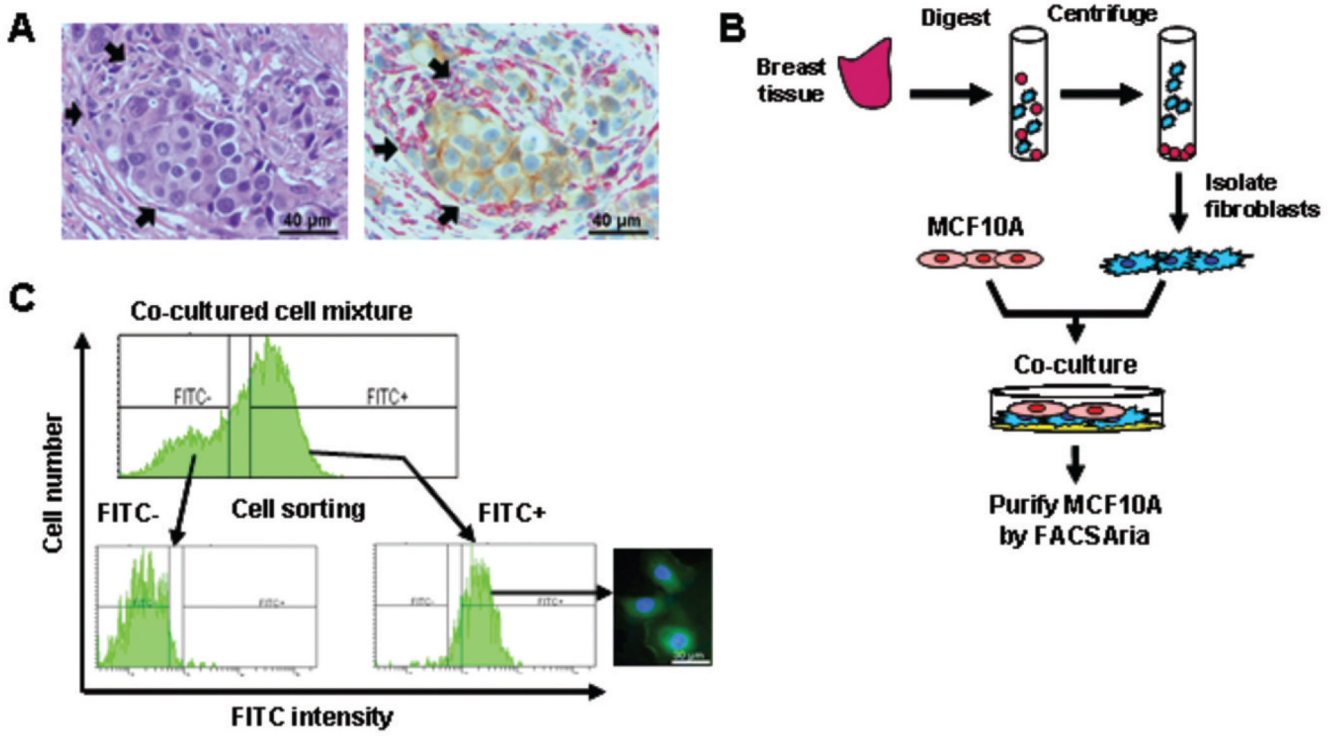

Figure 1.

Establishment of a co-culture system to simulate the breast tumor microenvironment. *A*, representative photographs demonstrate the close proximity between breast epithelial cells and stromal fibroblasts. Left panel: Hematoxylin and eosin staining of cancer tissue section. Right panel: Dual immunohistochemical staining of epithelia (β-catenin, brown) and fibroblasts (vimentin, red). Arrows indicate close contact between the two cell types. *B*, a flow chart summarizes the combinatorial culture experiment used in this study. *C*, isolation of MCF10A cells co-cultured with fibroblasts was carried out by flow sorting using FITC-conjugated anti-ESA antibody. Purities of the re-isolated cells were confirmed by immunofluorescence staining as shown in the inserted photograph.

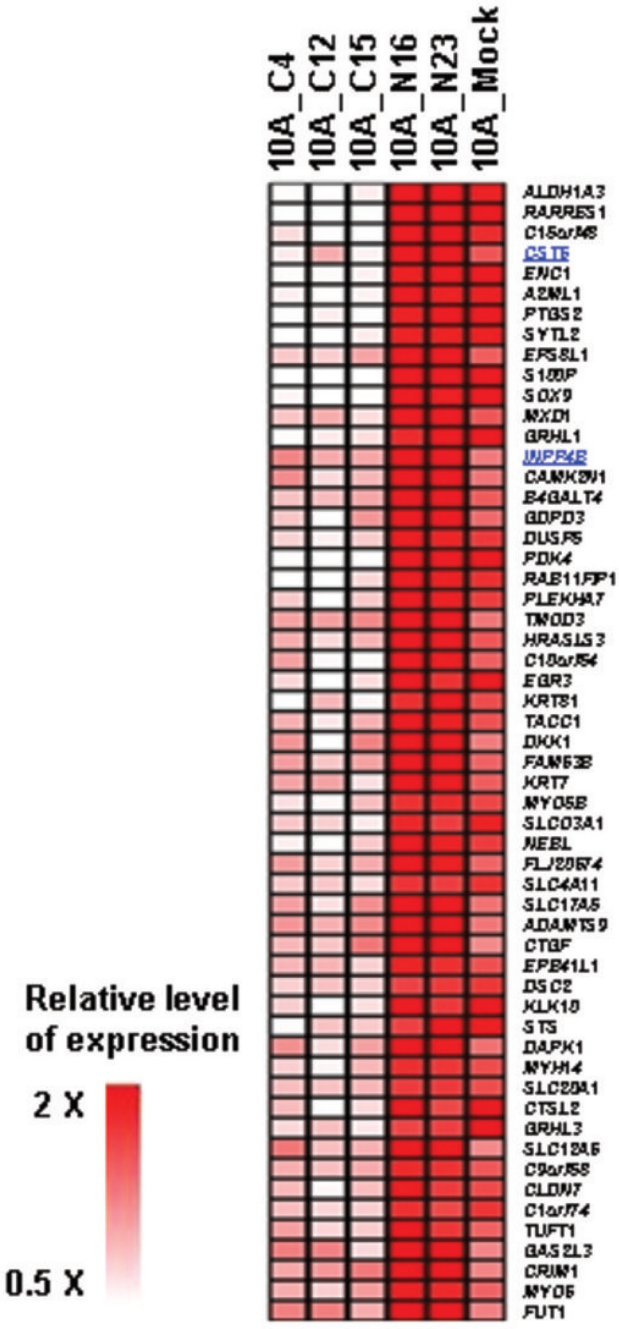

Figure 2.

Concurrently down-regulated genes in MCF10A cells exposed to cancer–associated fibroblasts (CAFs). The 56 genes, harboring CpG islands, are shown in heat map. After co-cultured with CAFs, MCF10A cells (10A_C4, 10A_C12, and 10A_C15) were subjected to RNA extraction followed by gene expression analysis using the Affymetrix U133 plus 2.0 system. Expression profiling was also conducted in MCF10A cells (10A_N16 and 10A_N23) co-cultured with normal fibroblasts and in a control (10A_Mock) not exposed to fibroblasts. An additional list of 109 down-regulated genes, including those shown in the heatmap (*n*=56), is provided in Supplementary Table S2.

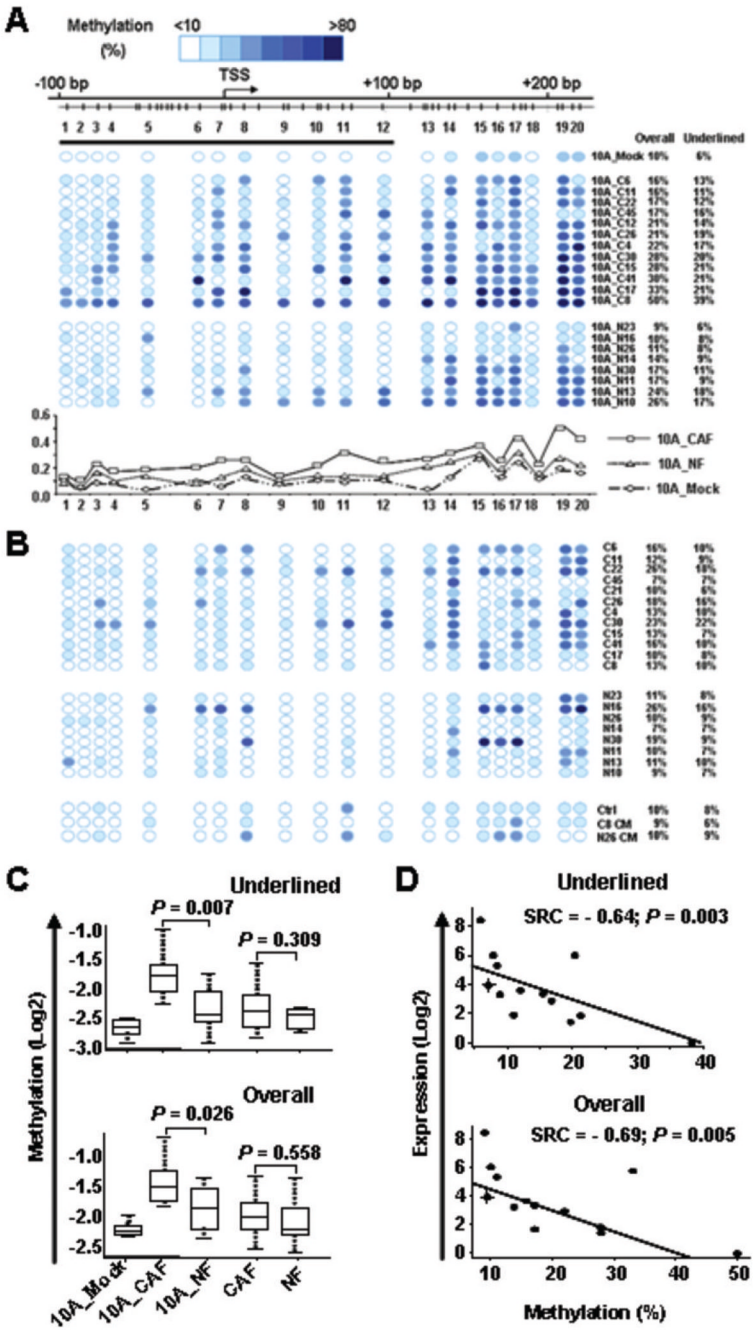

Figure 3.

Methylation mapping and gene expression analyses of the *CST6* CpG island in co-cultured MCF10A cells. *A*, twenty co-cultured MCF10A samples were subjected to the MassARRAY analysis as described in the text. Top: A genome map showing the locations of CpG sites and the transcription start site (TSS) of *CST6*. Middle: A methylation map derived from the MassARRAY analysis. Note that this assay will analyze multiple CpG dinucleotides together as a group if the sites are situated in close vicinity and within a digested fragment. Names of co-cultured samples and the average methylation levels of either the first 12 CpG units (underlined) or all 20 sites (overall) are shown at the right. Bottom: The landscape plots reveal greater levels of methylation in MCF10A cells co-cultured with cancer-associated fibroblasts

(10A_CAF) than in cells co-cultured with normal fibroblasts (10A_NF) or a mock control (10A_Mock). *B*, upper and middle panels: Methylation levels of the *CST6* CpG island in 20 monotypic fibroblasts (without MCF10A cells) were quantified. Lower panel: MassARRAY was used to assess the methylation levels of the *CST6* CpG in MCF10A cells after the exposure to conditioned media obtained from cancer-associated (C8 CM) or from normal (N26 CM) fibroblast culture. *C*, box-plots summarize the methylation level of the overall (low) or the first 12 CpG units (upper) in MCF10A_Mock control, co-cultured MCF10A cells and monotypic breast fibroblasts. *D*, inverse correlation between methylation and expression levels of *CST6*. The MCF10A_Mock sample was plotted as the cross in the figures.

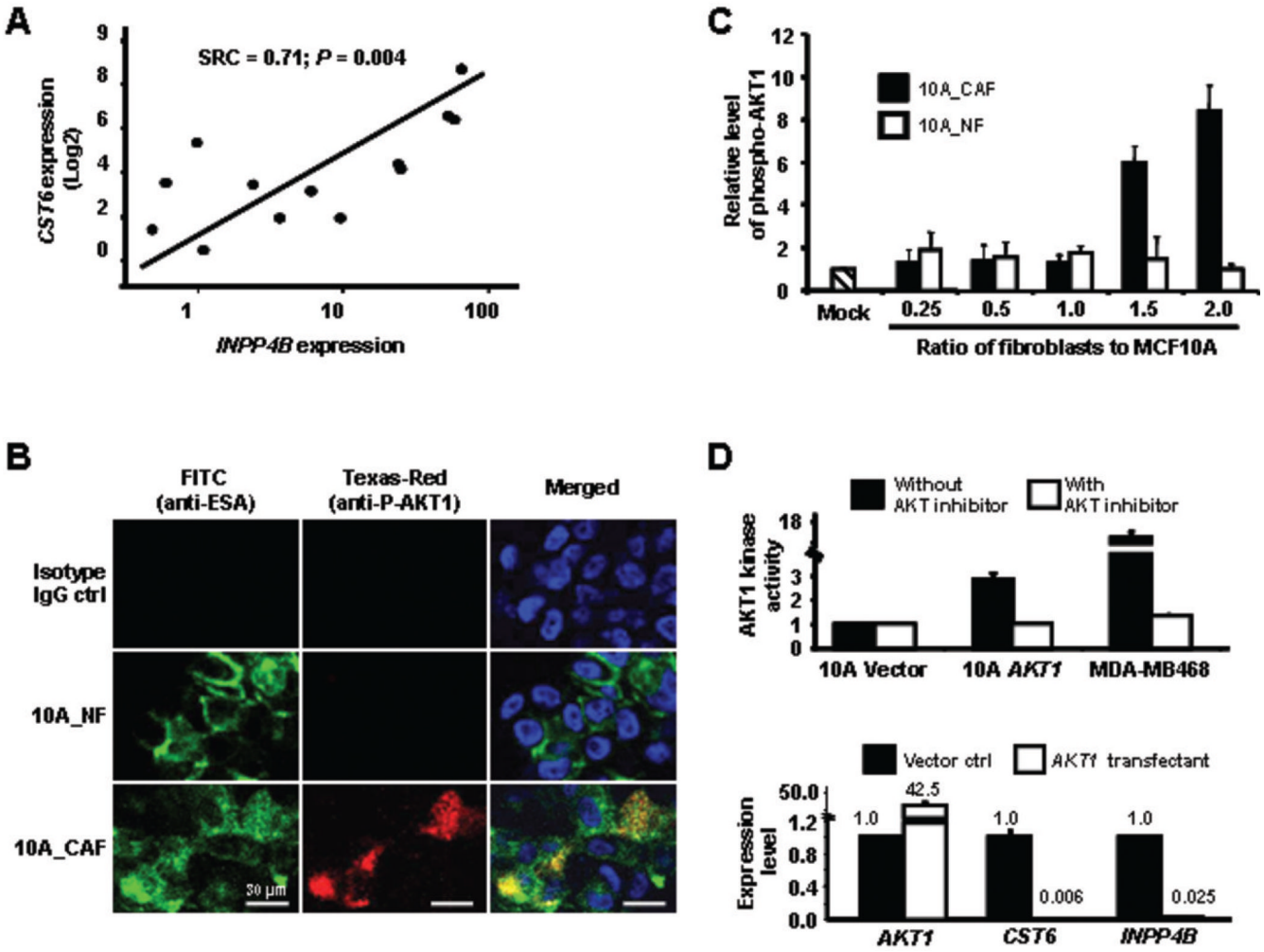

Figure 4.

Epigenetic silencing of *CST6* was induced by activated AKT1 signaling. *A*, positive correlation between the expression of *CST6* and *INPP4B* in MCF10A cells co-cultured with various breast fibroblasts was shown. Logistic regression analysis was performed and spearman rank coefficient (SRC) was calculated. *B*, the co-cultured MCF10A cells were fixed and dually immunostained with anti-phospho-AKT1 (Texas-Red) and anti-epithelial specific antigen (FITC, green) followed by a nuclear staining with DAPI (blue). Representative images from confocal cross sections are shown. *C*, influence of cancer-associated fibroblasts on MCF10A cells was assessed by elevated phospho-AKT1 kinase in the latter cells. Fibroblasts and MCF10A cells were mixed in various ratios (shown in the *x*-axis) and grown on the Matrigel-coated chamber slides. Two weeks later, dual immunofluorescence (IF) staining was carried out, and the resultant mages were captured and analyzed as described in the text. The basal level of phospho-AKT1 kinase (red) signals detected in the mock control experiments was arbitrarily defined as 1. An average value of 15 images with +/− SD from 3 independent assessments is shown for each co-culture set. *D*, MCF10A cells were transfected with either an empty vehicle (vector ctrl) or with pCDNA3 encoding a constitutively active myristylated form of *AKT1*. Upper, AKT1 kinase activities in transfectants and in a positive control cell line (MDA-MB468) were measured in the absence (black bars) or presence (white bars) of an AKT1 kinase inhibitor. Data represented an average of 3 independent AKT1 kinase assessments.

Lower, Expression levels of *AKT1*, *CST6* and *INPP4B* in transfectants were measured by quantitative RT-PCR.

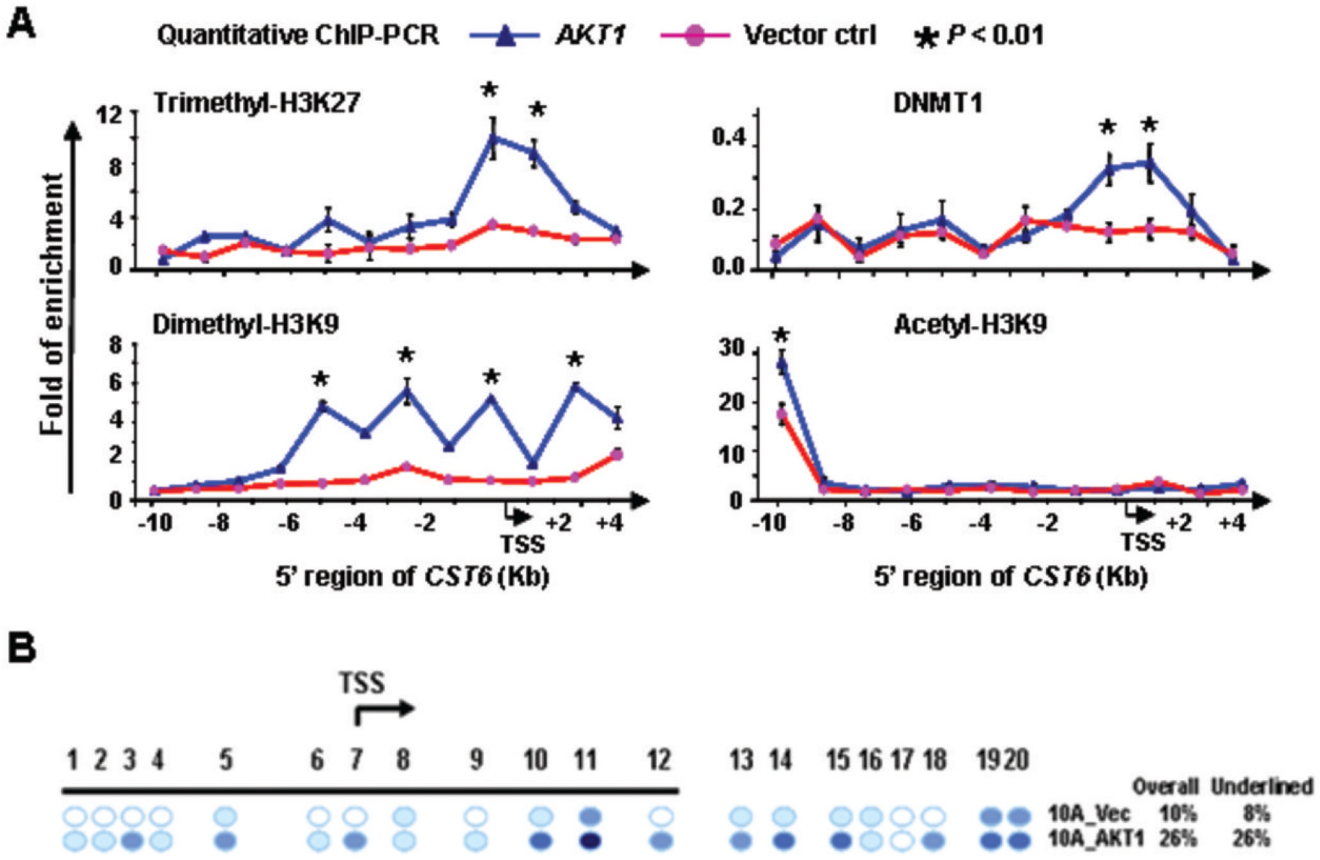

Figure 5.

Repressive chromatin marks enriched at the *CST6* locus. *A*, quantitative chromatin Immunoprecipitation (ChIP)-PCR analysis in *AKT1* transfected and control MCF10A cells was shown. Enrichment levels of 3 histone marks, trimethyl-H3K27, dimetyl-H3K9, and acetyl-H3K9 and DNA methyltransferase 1 (DNMT1) were analyzed in the *CST6* promoter and its surrounding regions (~15-kb). Data represented the average of 2 independent experiments. *B*, methylation analysis of the *CST6* CpG by the MassARRAY analysis in *AKT1*-transfected MCF10A and vector control cells. Representative data were derived from at least 2 independent transfectants.

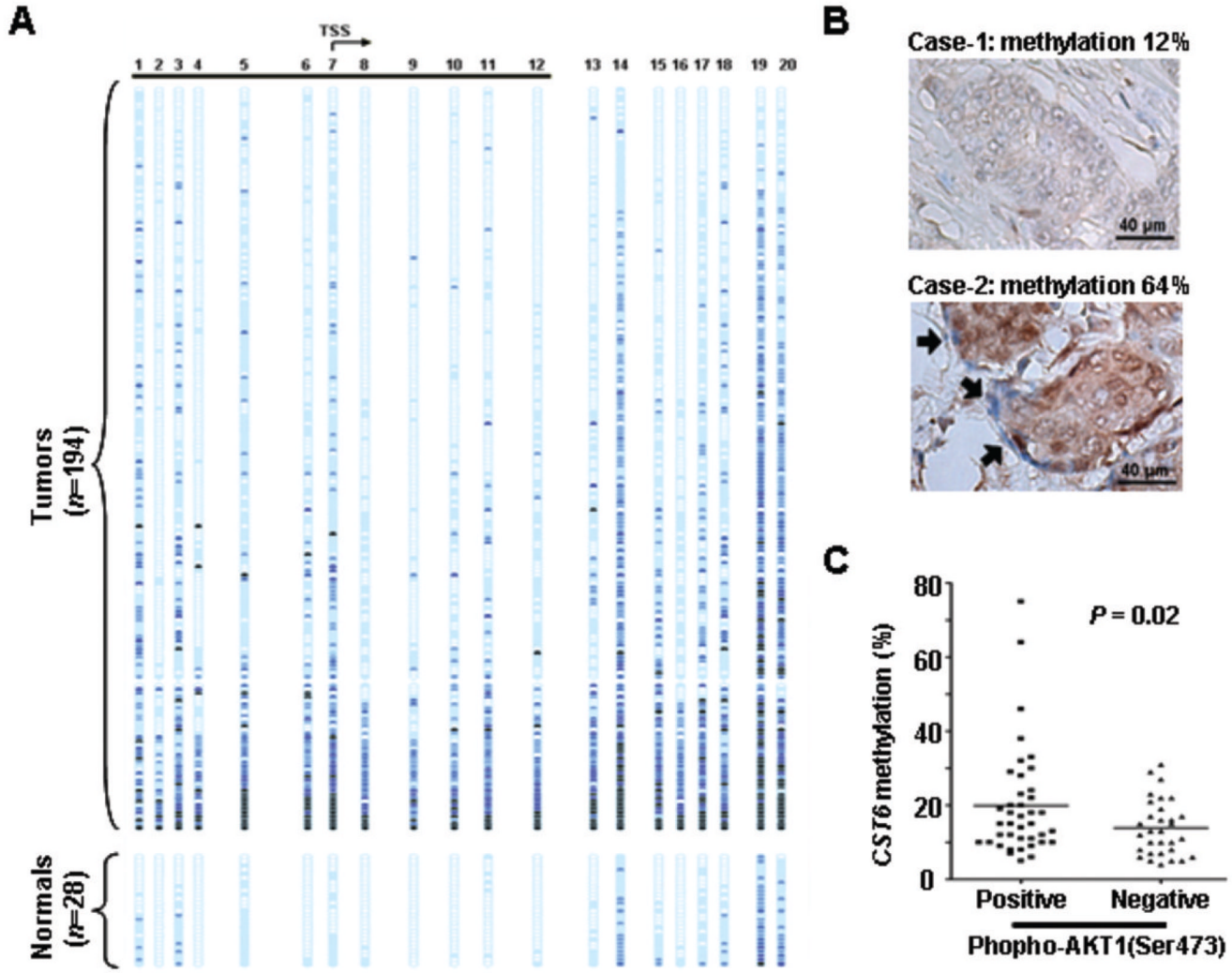

Figure 6.

Methylation analysis of *CST6* and immunostaining of phospho-AKT1 in primary breast tumors. *A*, methylation profiles of 194 primary breast tumors (upper) and 28 normal breast tissues (lower) were shown. The MassARRAY analysis was used to determine the methylation level of each sample. The methylation difference between cancer and normal tissues was determined to be significant in the overall ($p < 10^{-6}$) or the underlined ($p < 10^{-6}$) region (*t*-test). *B*, representative examples of differential expression of phospho-AKT on breast cancer tissue sections (Case 1: weak or undetectable with score 0; Case 2: strong with score 4, see Experimental Procedures for explanation). Arrows indicate tumor stromal cells that are in close contact with cancer epithelia. *C*, dot-plots indicate that the level of *CST6* promoter methylation is positively correlated with the phospho-AKT1 staining intensity in 72 primary tumors available for analyses. The horizontal bars indicate mean values. Significance of differences in methylation was determined by student *t*-test.